REPORT DOCUMENTATION PAGE

Form Approved
OMB No. 0704-0188

1. REPORT DATE *(DD-MM-YYYY)*	2. REPORT TYPE	3. DATES COVERED *(From - To)*
2011	Journal Article-Journal of Applied Physiology	

4. TITLE AND SUBTITLE

A physiological systems approach to modeling and resetting of mouse thermoregulation under heat stress

5a. CONTRACT NUMBER

5b. GRANT NUMBER

5c. PROGRAM ELEMENT NUMBER

6. AUTHOR(S)

B. Grossman, O.S. Shaik, B.G. Helwig, L.R. Leon, F.J. Doyle

5d. PROJECT NUMBER

5e. TASK NUMBER

5f. WORK UNIT NUMBER

7. PERFORMING ORGANIZATION NAME(S) AND ADDRESS(ES)

Thermal and Mountain Medicine Division
U.S. Army Research Institute of Environmental Medicine
Natick, MA 01760-5007

8. PERFORMING ORGANIZATION REPORT NUMBER

M10-23

9. SPONSORING/MONITORING AGENCY NAME(S) AND ADDRESS(ES)

Same as #7 above.

10. SPONSOR/MONITOR'S ACRONYM(S)

11. SPONSOR/MONITOR'S REPORT NUMBER(S)

12. DISTRIBUTION/AVAILABILITY STATEMENT

Approved for public release; distribution unlimited.

13. SUPPLEMENTARY NOTES

14. ABSTRACT

Heat stroke (HS) is a serious civilian and military health issue. Due to the limited amount of experimental data available in humans, this study was conducted on a mouse mathematical model fitted on experimental data collected from mice under HS conditions, with the assumption there is good agreement among mammals. Core temperature (Tc) recovery responses in a mouse model consist of hypothermia and delayed fever during 24 h of recovery that represent potential biomarkers of HS severity. The objective of this study was to develop a simulation model of mouse Tc responses and identify optimal treatment windows for HS recovery using a three-dimensional predictive heat transfer simulation model. Several bioenergetic simulation variables, including nonlinear metabolic heat production (W/m3), temperature-dependent convective heat transfer through blood mass perfusion (W/m3), and activity-related changes in circadian Tc were used for model simulation. The simulation results predicted the experimental data with few disparities. Using this simulation model, we tested a series of ambient temperature treatment strategies to minimize hypothermia and delayed fever to accelerate HS recovery. Using a genetic algorithm, we identified eight time segments (ambient temperature

15. SUBJECT TERMS

numerical modeling; heat stroke; hyperthermia; hypothermia; genetic algorithm

16. SECURITY CLASSIFICATION OF:			17. LIMITATION OF ABSTRACT	18. NUMBER OF PAGES	19a. NAME OF RESPONSIBLE PERSON
a. REPORT	b. ABSTRACT	c. THIS PAGE			L.R. Leon
Unclassified	Unclassified	Unclassified	Unclassified	8	19b. TELEPHONE NUMBER *(Include area code)* 508-233-4862

Reset

Standard Form 298 (Rev. 8/98)
Prescribed by ANSI Std. Z39.18

HIGHLIGHTED TOPIC | *Mechanisms and Modulators of Temperature Regulation*

A physiological systems approach to modeling and resetting of mouse thermoregulation under heat stress

Benyamin Grosman,[1,3]* Osman S. Shaik,[1]* Bryan G. Helwig,[2] Lisa R. Leon,[2] and Francis J. Doyle III[1,3]

[1]*Institute for Collaborative Biotechnologies, University of California, Santa Barbara, California;* [2]*Thermal and Mountain Medicine Division, United States Army Research Institute of Environmental Medicine, Natick, Massachusetts; and* [3]*Department of Chemical Engineering, University of California, Santa Barbara, California*

Grosman B, Shaik OS, Helwig BG, Leon LR, Doyle FJ 3rd. A physiological systems approach to modeling and resetting of mouse thermoregulation under heat stress. *J Appl Physiol* 111: 938–945, 2011. First published June 23, 2011; doi:10.1152/japplphysiol.00519.2010.—Heat stroke (HS) is a serious civilian and military health issue. Due to the limited amount of experimental data available in humans, this study was conducted on a mouse mathematical model fitted on experimental data collected from mice under HS conditions, with the assumption there is good agreement among mammals. Core temperature (T_c) recovery responses in a mouse model consist of hypothermia and delayed fever during 24 h of recovery that represent potential biomarkers of HS severity. The objective of this study was to develop a simulation model of mouse T_c responses and identify optimal treatment windows for HS recovery using a three-dimensional predictive heat transfer simulation model. Several bioenergetic simulation variables, including nonlinear metabolic heat production (W/m^3), temperature-dependent convective heat transfer through blood mass perfusion (W/m^3), and activity-related changes in circadian T_c were used for model simulation. The simulation results predicted the experimental data with few disparities. Using this simulation model, we tested a series of ambient temperature treatment strategies to minimize hypothermia and delayed fever to accelerate HS recovery. Using a genetic algorithm, we identified eight time segments (ambient temperature = 27, 30, 31, 29, 28, 28, 27, 26°C) of 110 min total duration that optimized HS recovery in our model simulation.

numerical modeling; heat stroke; hyperthermia; hypothermia; genetic algorithm

MAMMALIAN SPECIES HAVE DEVELOPED numerous mechanisms to cope with a wide variety of environmental stressors, including heat stress. Heat stress, which can progress to fatal heat stroke (HS) is a serious public and military health issue (16). HS results from prolonged exposure to a hot environment, causing core temperature (T_c) to exceed the normal temperature, leading to severe hyperthermia that can result in physical and cognitive function decrements. As such, HS is clinically characterized by hyperthermia (T_c typically, but not always greater than 40°C) collapse and profound encephalopathy that presents as delirium, agitation, stupor, seizures, or coma (6). Rapid cooling therapy and fluid resuscitation represent the current treatment strategies, but there are currently no effective pharmacological treatments for HS. Despite clinical cooling therapies that rapidly lower body temperature to minimize tissue injury, HS is often fatal and results in permanent neurological damage in 30% of survivors (3). Identification of novel therapies and optimal treatment windows to accelerate recovery are needed to minimize HS morbidity and mortality.

In the present study, we used a mathematical model to simulate mouse T_c responses during heat stress and recovery and identify optimal time windows for ambient temperature (T_a) treatment strategies to optimize resetting of the thermoregulatory profiles back to normal T_c. In the past three decades, several mathematical models of the human thermoregulation system have been developed to enhance understanding of regulatory processes (5, 9, 4a, 18). Most of these models were based on cylindrical approximations of the body segments with shell layers representing the body tissue layers. Due to the limited amount of experimental data available in humans and the inability to study T_c recovery responses in HS patients, it has not been possible to utilize these models to test the efficacy of treatment strategies during recovery. In this study, mouse T_c responses during heat exposure and 40 h of recovery were modeled to expand current prediction capabilities through several circadian cycles and test the efficacy of several T_a treatments on HS recovery.

Our laboratory recently developed an in vivo mouse HS model using conscious free-moving animals with implanted radiotelemetry devices to examine T_c responses through 48 h of HS recovery (14). This was the first in vivo HS model to remotely measure T_c through several circadian cycles without compromising the subject's natural behavioral and autonomic thermo-effector responses to prolonged heat exposure (14). Following heat exposure to a maximum T_c ($T_{c,max}$), ranging from 42.4 to 42.7°C, mice exhibited a biphasic thermoregulatory recovery response consisting of initial hypothermia followed by fever at 24 h (12, 13). Survival rates, depths of hypothermia, and recovery times of mice subjected to heat stress were mainly affected by $T_{c,max}$ attained during heat exposure, as well as recovery T_a.

MATERIALS AND METHODS

Mouse heat transfer mechanisms were modeled with consideration of conduction, convection, and radiation through the skin to the environment as a passive system. In addition, metabolic heat production, blood flow, saliva spreading, and shivering (referred to as the active controlled system) were addressed, in part, in our model. The passive system was modeled as multiple layers of tissue with distinct anatomical differences, and the active system was designed to be a function of the difference among multiple tissue temperatures and the desired set-point temperature (T_{set}). In homeothermic animals, main-

---

* B. Grosman and O. S. Shaik contributed equally to this work.

Address for reprint requests and other correspondence: F. J. Doyle III, Dept. of Chemical Engineering, Univ. of California, Santa Barbara, Santa Barbara, CA 93106–5080 (e-mail: doyle@engineering.ucsb.edu).

tenance of a relatively constant T_c is achieved by an increase in metabolic heat production and reduction in heat loss when $T_c < T_{set}$, and a reduction in metabolic heat production and an increase in heat loss when $T_c > T_{set}$ (21). The difference between the T_c of tissues and T_{set} serves as the driving force for heat transfer mechanisms.

Mouse geometry. Mouse geometry was idealized as an ellipsoid for the torso (length, 0.08 m, diameter, 0.003 m) and a cone for the tail (length, 0.075 m), with multiple tissue layers (skin, fat, muscle, core, and bone). The thickness of tissue layers (skin, fat, muscle, and core organs) was based on approximate percentage of the total body weight. Metabolically active components, including the brain, heart, liver, and kidneys, were considered in the core layer of the mouse torso. Trakic et al. (22) yielded a 25.7-g mouse voxel phantom with a resolution of $0.13 \times 0.13 \times 0.143$ mm^3 from similar $0.39 \times 0.39 \times 0.43$ mm^3 voxel phantom of a male Sprague-Dawley rat with a mass of $\sim$370 g. We used this approximation with volume of 3.65, 3.97, 4.41, and 4.50 mm^3 of the skin, fat, muscle, and stomach layers, respectively. Volumes of brain, heart, liver, and kidneys were calculated from the preceding voxel data, and equivalent volumes of spheres were considered in the model. The software package Comsol Multiphysics was used to define the geometry and mesh the model. Input variables included initial conditions of the mouse T_c, global expressions (Comsol types of expressions that are used by different domains of the model), and boundary conditions, along with material properties. Comsol uses an adaptive finite-element-based method to solve the resulting partial and ordinary differential equations. To minimize the computational costs, a symmetric problem with one-half of the actual geometry was implemented.

The model included the major heat transfer mechanisms of conduction, radiation, blood perfusion, metabolic heat production, evaporation, and convection. The temperature distribution inside the tissue was computed by the Pennes bio-heat transfer equation (BHTE) (17). The differential equation that describes the heat dissipation in a homogenous, infinite tissue volume was given by the following Pennes BHTE (7):

$$\rho(\zeta)C_p(\zeta)\frac{\partial T(\zeta, t)}{\partial t} = K(\zeta)\nabla^2 T(\zeta, t) + B(\zeta, t) + Q(\zeta, t) + Q_r(\zeta, t) \quad (1)$$

where $\zeta = (x, y, z)$, ρ (kg/m^3) is the specific mass density, C_p (J·kg^{-1}·°C^{-1}) is the specific heat, T (°C) is the temperature at time t, K (W·m^{-1}·°C^{-1}) is the thermal conductivity, B (W/m^3) is the convective heat exchange between blood and tissue, Q (W/m^3) is the metabolic heat generation, and Q_r (W/m^3) is thermal radiation governed by the Stefan-Boltzmann law. Pennes postulated that the total heat exchange between the blood and the surrounding tissue could be modeled as a nondirectional heat source whose magnitude is proportional to the volumetric blood flow and the difference between the local tissue temperature and the blood temperature (17). Blood enters each tissue compartment at the temperature of the central blood compartment and returns to the central compartment at the current tissue temperature. The central circulatory system is conceptual and actually simulates the blood system as a single compartment, in which blood from various organs is mixed, then redistributed. The rate of heat transfer by blood flow through different tissue layers is modeled as a response to the physiological demands and thermoregulation (22).

Blood perfusion rates to different tissues is temperature dependent at the space time point, which is controlled by combinations of global signals (depending on temperature receptors throughout the whole body, integrated in the hypothalamus) and local signals. The blood perfusion equilibrium rate is assumed to double for each 4.5°C rise in temperature $T(\zeta, t)$ (2). The equilibrium is assumed to be reached exponentially by the following time-dependent equation (23):

$$\frac{\partial \omega_x}{\partial t} = \frac{1}{\tau_{blood}}\{\omega_{x,0}\exp[\alpha(T - T_0)] - \omega_x\} \quad (2)$$

where ω_x and $\omega_{x,0}$ (m^3·kg^{-1}·s^{-1}) are dynamic and basal blood perfusion [estimated from Trakic et al. (22)] for a specific organ-tissue x, respectively; τ_{blood} is time constant (12 min); and $\alpha = \ln(2/4.5)$°C^{-1}.

Metabolism. Resting energy expenditure (REE) or basal metabolic rates are expressed as a function of mammalian body mass, according to Kleiber's law (24). An organ-tissue level REE model is formulated for metabolically active organs, such as the liver, heart, brain, kidneys, and remaining tissues. Among all mammals, the brain, liver, kidneys, and heart account for 73% of total REE (4). The equations for metabolically active organs and remaining tissues are based on Wang et al. (24)

$$Q_{bas,x,0} = \alpha_x \cdot M^{-\beta_x} \cdot 2^{T_x \frac{-T_{set}}{10}} \quad (3)$$

where $Q_{bas,x,0}$ (W/m^3) is the basal metabolic heat production of the organ-tissue x, M (kg) is the body mass of the mammal, α_x and β_x are specific constants of the organ x, and T_x is the organ-tissue temperature (22). In endotherms, the dependence of biochemical reactions on temperature is described by the van't Hoff Q_{10} effect (24) with a sensitivity coefficient of 2.

In addition to blood perfusion rates (Eq. 2), thermoregulatory responses consisted of metabolic heat production that was based on integrating the error between T_c and T_{set}, given by the following equations:

$$Q_{bas,x}(\zeta, t) = Q_{x,bas,0} \cdot M_r$$

$$\frac{dM_{r1}}{dt} = k_m(T_{set} - T_c)$$

$$M_r = \begin{cases} M_{r1} & M_{r,low} < M_r < M_{r,up} \\ M_{r,up} & M_{r1} > M_{r,up} \\ M_{r,low} & M_{r1} < M_{r,low} \end{cases} \quad (4)$$

where M_{r1} is the metabolic regulation factor, which is driven by the deviation between T_c and T_{set}, M_r is the constraint metabolic regulation factor, and k_m (°C^{-1}·s^{-1}) is an empirical gain. The M_r value is bounded between $M_{r,low}$ and $M_{r,up}$, the lower and upper constraints to the metabolic regulation factor, respectively. The values of k_m can differ from organ to organ and for different tissues; however, for the present case, due to lack of biological data, it is assumed to be equal for all tissues and organs in the mouse body. The exact mechanism of the metabolic regulation is unknown, but we assumed that, after a prolonged heat load, the body is trying to minimize metabolic activity. On the other hand, when the body temperature is low for a prolonged time, M_r can get the value of $M_{r,up}$. This resembled a constraint integrator in process control. Notice that M_r is a multiplier on the temperature-dependent metabolic function, as shown in *Eq. 5*.

The metabolic heat production of the muscle tissue is given by the sum of the basal value $Q_{bas,x}$ and the additional heat ΔQ_m, which may be produced by local autonomic responses, such as normal activity and/or shivering thermogenesis:

$$Q_x(\zeta, t) = Q_{bas,muscle} + \Delta Q_m$$

$$\Delta Q_m = Q_{bas,muscle} \cdot \frac{activity}{100} \quad (5)$$

where the change in basal metabolism, ΔQ_m, is the difference between the actual basal rate and the basal rate corresponding to neutral thermal conditions, and activity is measured as number of gross motor movements per minute. Factors, including the rate of movement, can affect activity readings; thus reported activity should be considered a relative value and does not provide insight regarding the absolute distance the animal moved. Activity was simultaneously collected for

each animal throughout the data collection period and reported by the data analysis software on a per-minute basis following collection of T_c values. We calculated the correlation coefficient between activity and oxygen consumption on 570 experimental data points (12) and found it to be 0.54 (P value of 2e-46), meaning that there is a significant correlation between metabolic rate and mouse activity.

Circadian variation in T_c is modeled by considering the activity levels of mice and the drinking of water at 25°C (25). An additional heat term, $Q_{m,a}$, is added to the muscle layer and other metabolically active organs to account for the increase in T_c due to activity levels. Heat is lost in the core layer of the mouse body due to the drinking of 25°C water. This amount of heat ($Q_{m,w}$; J/m³) is removed from the core layer of the mouse body based on following equation:

$$Q_{m,w} = \rho_w \cdot C_{p,H_2O}(T_{average} - T_{amb}) \cdot \frac{V_{water}}{V_{stomach}} \quad (6)$$

where ρ_w (kg/m³) is the density of the water consumed by the mouse, C_{p,H_2O} (J·kg^{-1}·°C) is the specific heat of water, V_{water} is the amount of water consumed (m³), and $V_{stomach}$ is the volume of the stomach (m³).

Heat is exchanged from the mouse body by convection with the ambient air (Q_c; W/m²), by water evaporation due to saliva spreading on the skin or fur surface (Q_e; W/m²), and by respiratory losses (Q_{rp}; W/m²). The rate of heat exchange over the body of the mouse varies, with regard to the furred torso and the unfurred appendages. Hence, heat balances from furred torso and unfurred tail are modeled as different boundary conditions. In general, the net heat flux Q_s (W/m²) exchanged from the surface of the body is equivalent to the sum of these individual heat exchanges ($Q_s = Q_c + Q_e + Q_{rp}$). The heat loss due to forced convection is governed by the equation:

$$Q_c(\zeta, t) = -h[T(\zeta, t) - T_a] \quad (7)$$

where $Q_c(\zeta,t)$ (W/m²) is the convective heat loss, h (W·m^{-2}·°C^{-1}) is the convective heat transfer coefficient, T_a is in °C. In this work, h is evaluated by the empirical formula given by Wooden and Walsberg (26). Different values of h are used for the furred torso and the tail (h is larger by 25% on the tail). When $T_c < T_{set}$, mice piloerect their fur to create an extra layer of insulation, thereby conserving body heat. In contrast when $T_c > T_{set}$, as was present in the present study, mice relax the piloerection response to facilitate heat loss to the surroundings. This behavioral response was incorporated into the model by using h as a linear function of average temperature on the torso (*Eq. 8*) that results in $h = 3$ W·m^{-2}·°C^{-1}, when $T_c = T_{set}$.

$$h = (T_c - 10)/9(W \cdot m^{-2} \cdot °C^{-1}) \quad (8)$$

In rodents, the behavioral spreading of saliva on the ventral body surfaces is an essential mechanism for heat loss through water evaporation. Q_e represents evaporative heat transfer rate per unit area and consists of passive diffusion and evaporation of saliva. Passive diffusion is a small quantity of residual mass transfer that occurs between skin and surroundings, which is negligible in the present case. Mouse T_c increases when sufficient heat cannot be transferred to the environment by the normal heat loss mechanisms of convection, conduction, diffusion, and radiation. The result is an increased T_c above T_{set}, triggering the active thermoregulatory control system of saliva spreading. When exposed to heat stress near 40°C, rodents exhibit a peak in evaporative heat loss; however, when exposure continues, the evaporative heat loss falls rapidly in hamsters, whereas in rats it is maintained for several more hours before heat exhaustion occurs (7). Due to lack of data available for mice, the salivation profile is set by optimization to best fit the experimental data, and it is triggered by the active system once the heating begins. Evaporative heat loss is represented by the following differential equation:

$$Q_e = \frac{\lambda_{H_2O}}{A_{sl}} \frac{dm_s}{dt} \quad (9)$$

where A_{sl} (m²) is the salivary evaporation skin surface; m_s is amount of saliva spreading; and $\lambda_{H_2O} = 2,256 \times 10^3$ J/kg is the heat of evaporation of water. In the present work, only the front ventral part of the mouse body and front legs are considered as A_{sl}. Evaporative heat loss becomes greater as the gradient temperature between T_c and T_a increases, albeit it reduced, after the dehydration point is reached, eventually becoming ineffective as the remaining saliva on the body surface evaporates. The time corresponding to the point of dehydration (t_d; s), duration (μ; s), and the maximum amount of saliva spreading ($m_{s,max}$; kg/s) at any time during heat stress are parameters that differ from mouse to mouse. The exponential expression that represents the heat loss due to saliva spreading is described by *Eq. 10*.

$$Q_e = \frac{\lambda}{A_{sl}} m_{s,max} e^{-\left(\frac{t \, t_d}{\mu}\right)^2} \quad (10)$$

Respiratory heat losses occur when air is inhaled at T_a and exhaled close to T_c with high humidity. In Schmidt-Nielsen et al. (20), it is discussed that, in small rodents (Kengero rat), the mechanism of heat loss through respiration is highly efficient, and, therefore, it can be approximated to be zero. Therefore, in the present model, we do not define the pulmonary tract as a separate organ, and the respiratory heat losses are neglected.

RESULTS

The mathematical model in the preliminary stage needs to be calibrated to the experimental data. The following parameters were left as degrees of freedom and were determined with the help of optimization [genetic algorithm (GA)]: the time corresponding to the point of dehydration (t_d; s), the salivation duration (μ; s), the maximum amount of saliva spreading ($m_{s,max}$; kg/s^1), T_{set} in the experimental starting time, the lowest value of metabolic regulation factor ($M_{r,low}$), the empiric gain k_m (*Eq. 4*), and M_{r0} (the initial value of *Eq. 4*). Table 1 specifies results of the optimization and the parametric range in which the optimization search was done.

T_{set} was selected as a parameter in the calibration of the model because the mice showed decreasing T_c before heat stress [i.e., during transition into the lights-on (inactive) period], which was explicable as a change in T_{set}. The parameters of the salivation (t_d, μ, and $m_{s,max}$) were chosen because of its large effect on mouse thermoregulation and the lack of exact measurements in this species. The salivation profile using the parameters that are presented in Table 1 predicts an overall salivation of 2.9 g over the 4 h of heating. The parameters of *Eq. 4* were calibrated due to a lack of experimental data

Table 1. *List of parameters used to calibrate the mathematical model to the experimental data*

Parameter	Range	Value
t_d, s	2,400–6,000	4,425
μ, s	6,667–20,000	1.0667e + 004
$m_{s,max}$, kg/s	1.3312e−007–3.3280e−007	2.4545e−007
T_{set}, °C	32–38	35
$M_{r,low}$	1–2	1.625
k_m, °C^{-1}·s^{-1}	1e−5–4e−5	2.875e−5
M_{r0}	2–3	2.6875

Shown are the parameter denomination, range of optimization search, and final optimization value. See text for definition of parameters.
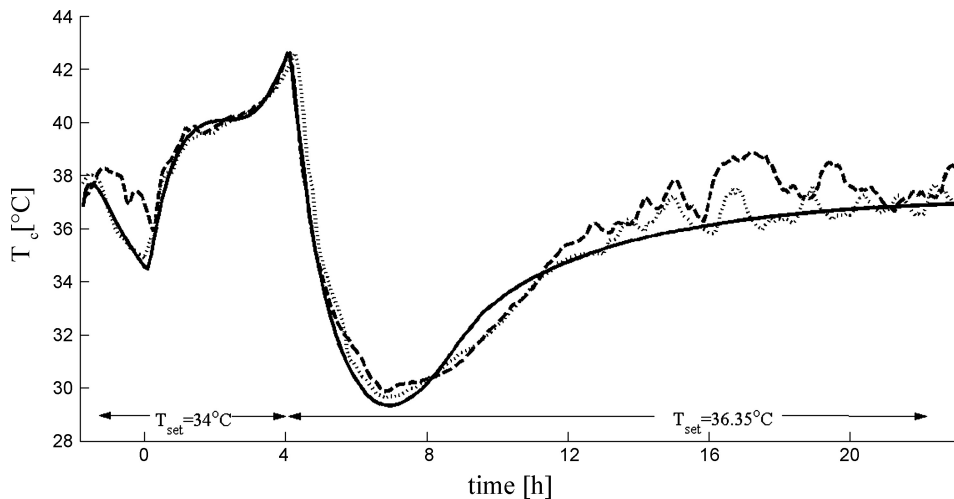
Fig. 1. The mathematical model response vs. two experimental data. The figure depicts the good agreement of the mathematical model (solid line) to two curves of empirical data (dotted and dashed lines). To calibrate the mathematical model to the experimental data, seven parameters were adapted using optimization. The typical behavior that is observed in the stage of the heating is controlled by regime of the salivation in combination with set-point temperature (T_{set}) that is fixed for 34°C. T_c, core temperature.

describing the function that regulates metabolic activity in the presented mathematical model; however, the value of k_m can be approximated by the speed of the regulation that was observed in the experiments.

Figure 1 shows the successful agreement between the calibrated mathematical model and the experimental data. The variation of T_c using $T_{set} = 34$°C from the beginning of the simulation until the mouse is removed from the heat chamber (4 h), and $T_{set} = 36.35$°C for the rest of the simulation, results in a very good agreement with the experimental data. The constrained metabolic regulation factor (M_{r1}) dynamic behavior is depicted in Fig. 2. We predicted that, in order for the mouse to achieve homeostasis, the metabolic heat production that is predicted by Kleiber's law (known to change between different species) should be multiplied by approximately three. Moreover, under heat stress, the mouse was predicted to reduce its metabolic heat production by ~50%. We predict that the main reason hypothermia occurred during recovery was due to a reduction in metabolic activity, which did not show a reversal for several hours.

A coarse mesh of the mouse model can be seen in Fig. 3. As a first case, a passive cooling scenario was simulated without considering the additional heat production and blood perfusion terms in the overall BHTEs. At the end of HS experimentation,

a subset of mice ($N = 4$) was killed and placed into a preheated environmental chamber until a T_c of 42.7°C was attained. Following this heating paradigm, mice passively cooled at T_a of 25°C for 60 min. Simulation results of the computational model are compared with these experimental passive cooling data in Fig. 4. T_c profiles of the simulated model reached $T_c = 32$°C from $T_c = 42.7$°C slowly compared with experimental data for passive cooling. Sensitivity analysis of the model with respect to parameter h was performed by varying ±20% of its nominal value of $h = 3.5$ W·m^{-2}·°C^{-1}. By increasing and decreasing the value of h, passive cooling times were decreased and increased, respectively; however, the deviation of T_c from the nominal cooling curve was not significant. Sensitivity analysis of the model was also carried out with respect to scaling of the mouse body. Whole mouse geometry was scaled by ±10% from its nominal size; mice with 10% reduction in scale showed similar passive cooling profiles to those from the experiments. The nominal mouse geometry was updated with a 10% reduction in size, and the new dimensions were used for further calculations.

The spatial temperature distribution across a mouse body for the hyperthermia region at $t = 200$ min is shown in Fig. 5. When exposed to $T_a = 39.5$°C, the tail temperature rose quickly due to increased skin blood flow to a heat-dissipating
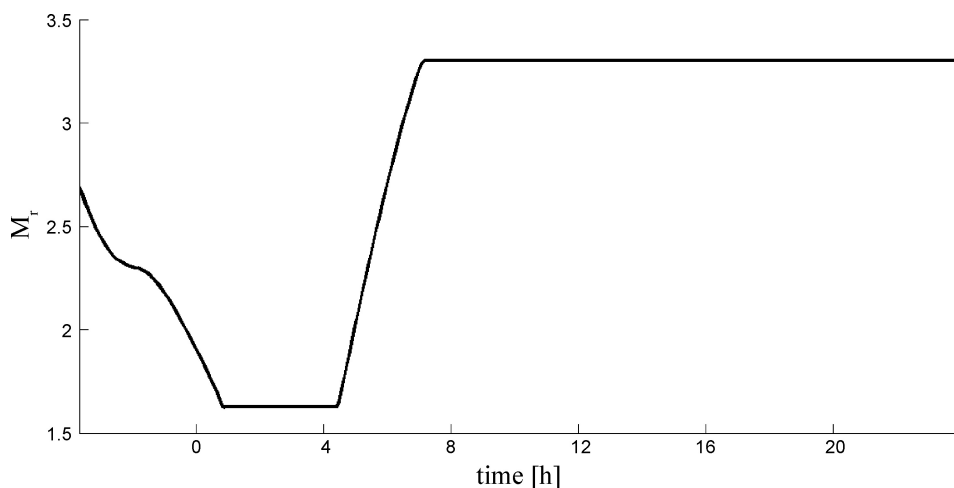

Fig. 2. Variability of the constrained metabolic regulation factor (M_r) during stage of the preheating, the heating, and the acclimatization periods. During the heating and in the early stage of the acclimatization, M_r reach the lower bound; later it takes M_r around 3 h to arrive to its upper bound, while recovering from the hypothermia.
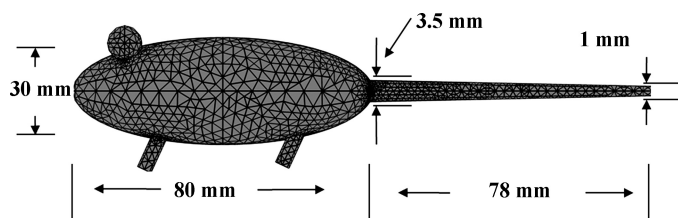
Fig. 3. A three-dimensional computational mouse geometry with torso and tail is shown. Dimensions of the torso and tail are taken from average experimental measurements of mice subjected to heat stress. The torso consists of four layers: skin, fat, muscle, and core. The tail layer consists of core and skin. Metabolically active organs, heart, liver, brain, and kidney, are considered spheres in core layer of the torso. Only one-half of the mouse geometry is used in the computational domain due to symmetry of the mouse body around the center and to minimize computational cost. A finite-element mesh with 44,267 nodes is generated for the computational mouse model in Comsol.

Fig. 5. Distribution of temperature across a mouse body under heat stress at ambient temperature (T_a) = 39.5°C. Plot corresponds to time t = 200 min under hyperthermia region. A minimum temperature of 15°C is observed on the front legs due to salivary evaporative heat loss.

organ with a larger surface area-to-volume ratio and higher h value. Heat loss due to spreading of saliva on the front ventral part and feet of the mouse body were observed in the surface plots. A maximum temperature gradient of 23°C was observed from the center of the body surface to front legs due to evaporative heat loss from spreading of saliva. On average, the front part of the mouse body was exposed to lower temperatures compared with the tail and center part of the body, where liver, kidneys, and intestines reside. Within the hyperthermia region, temperatures of these organs were more than the actual mouse T_c, suggesting these internal organs were more susceptible to thermal injury. Also, due to the high metabolic activity in the liver, the average liver temperature is assumed to be more than the mouse T_c observed in simulations.

The three-dimensional thermoregulation model was used to optimize the recovery time of a heat-stressed mouse, by varying T_a in the hypothermia region. T_a was optimized in the control region consisting of eight 110-min segments, totaling 880 min of initial recovery region. These control regions in the time domain were initialized after the desired $T_{c,max}$ = 42.4°C was attained in the hyperthermia region under heat stress. The optimal T_a zone was followed by a constant T_a =25°C for the rest of the simulation time. A GA optimization (10) was used to minimize a given cost function in *Eq. 11*.

$$V = \frac{err_+^T err_+ \cdot 10 + err_-^T err_-}{N} \qquad (11)$$

where V is the value of the cost function, err_+ is the residual of the T_c over T_{set}, err_- is the residual of T_c below T_{set}, and N is the number of recorded data points that were collected from the three-dimensional solution. The range of T_a that can be varied during the optimization is restricted to (21°C to 39°C). Five GA runs were conducted, with a population size of 10, and mutation of 5%. We kept members of previous generations when offspring performance was inferior. The termination criteria was 50 generations without change in the value of the cost function. This approach was presented in Grosman and Lewin (8). The optimized parameters were represented by four binary length numbers, which lead to the resolution of 1.2°C.

Figure 6*A* depicts a comparison of thermoregulatory profiles of heat-stressed mice recovering at T_a = 25°C with that of different T_a values obtained by GA solution and other suboptimal cooling profiles. The solution obtained by the GA optimizer (solid line A and B) to recover the T_c back to T_{set} suggested that, once a mouse reaches $T_{c,max}$, it should recover at T_a = 27°C for 110 min initially. In the second stage, the mouse should recover in a mildly heated environment of T_a = 30°C and T_a = 31°C for 220 min, followed by five 110-min segments at T_a = 29, 28, 28, 27, and 26°C, representing a gradual reduction of T_a. The GA solution for optimal cooling reduced the T_c after heat stress; however, once the T_c dropped below T_{set}, a moderate heating profile was applied to prevent prolonged hypothermia. The value of the cost function presented by *Eq. 11* obtained for this optimal solution was 3.8. The dotted lines in Fig. 6 (*A* and *B*) describe an alternative solution where the cooling profile started with initial 110 min at T_a = 21°C and then T_a = 25°C for the rest of the period. This solution resulted in a longer hypothermia region with a cost function value of 7.5. The dashed-dotted line in Fig. 6 (*A* and *B*) describes a cooling scenario, where the mouse was kept at T_a = 25°C throughout the recovery period, which resulted in slower temperature reduction after the hyperthermia and a slower recovery from the hypothermia with the cost function
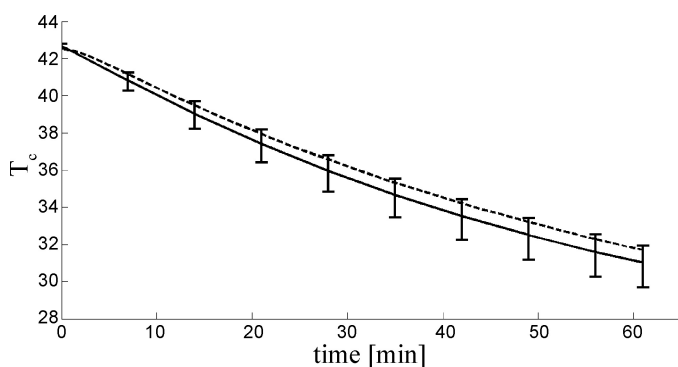

Fig. 4. Comparison of passive cooling rates in dead mice. The plot shown here compares the experimental cooling rates (solid line) with the computational mouse model (dashed line). Experimental cooling curves of 4 different mice are plotted around the mean values. Starting with the same initial temperature of 42.7°C, the error bar represents the minimum and maximum values of temperature in different mice during cooling.
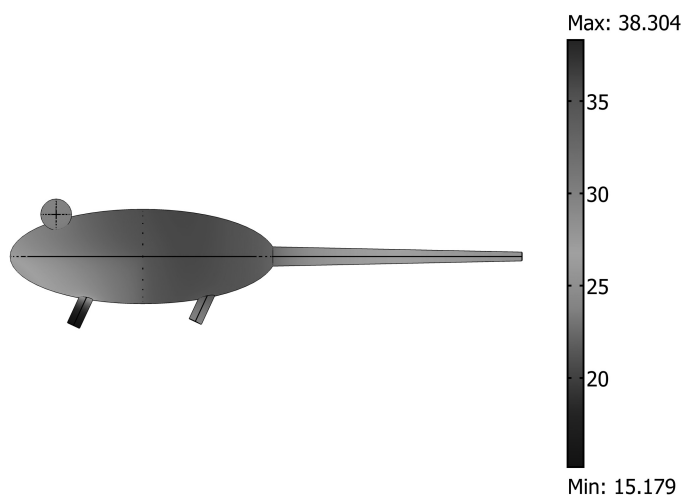
A

Legend:
— 27 30 31 29 28 28 27 26
······ 21 25 25 25 25 25 25 25
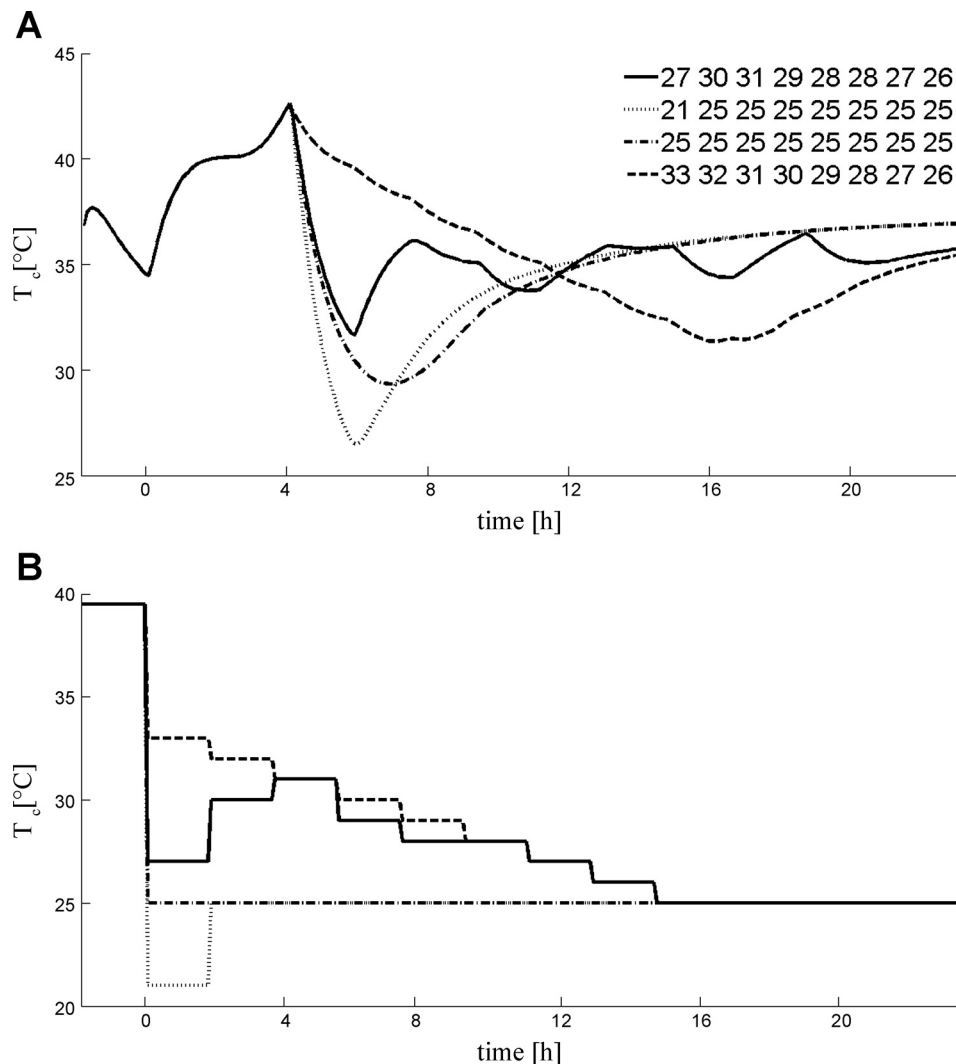—·— 25 25 25 25 25 25 25 25
--- 33 32 31 30 29 28 27 26

B

Fig. 6. Optimal T_a values obtained by genetic algorithm solution for recovering the mice T_c back to T_{set} are compared with suboptimal solutions and nominal solution after the maximum $T_c = 42.4°C$ is reached in 240 min. Thermoregulatory profiles of mice exposed to $T_a = 39.5°C$ during heat stress and recovering at $T_a = 25°C$ are shown in *A* with dash-dot line, and the corresponding T_a profile is shown in *B*. Mice T_c profile using optimal T_a obtained by genetic algorithm solution is shown in *A* by solid line, and the corresponding T_a controls are shown in *B*, which are compared with suboptimal solutions in dashed lines in both plots.

for this case of 6.5. In the last scenario, T_a was gradually reduced from $T_a = 33°C$ to 25°C, which resulted in a slower drop from hyperthermia with a cost function of 10.2. The T_c recovery time for a heat-stressed mouse from the hypothermia region with constant $T_a = 25°C$ was around 12 h. However, with optimal variable T_a, one can recover the mouse T_c back to T_{set} in around 7 h. In summary, the GA solution predicted that, to reduce the recovery period, the mouse should be cooled instantly after the hyperthermia; however, after the mouse T_c reaches a temperature around 32°C, a moderate heating period that gradually is reduced to $T_a = 25°C$ should be applied.

DISCUSSION

Heat exchange with the environment can have significant effects on thermal tolerance and HS recovery in mice. A mammalian thermoregulation model was designed to simulate heat stress and 24-h recovery profiles of mice with consideration of passive (conduction, convection, and radiation) and active systems. The passive system was developed using different thermophysical and physiological properties of tissue materials, and the active system based on a set point integral controller that simulates hypothalamic control of thermoregulation. Different heat transfer mechanisms, conduction, con-

vection, radiation, blood perfusion, evaporation, and metabolic heat production, are considered within tissues and the surroundings. The validity of the passive system was compared with passive cooling profiles of mice to more accurately simulate mammalian thermoregulatory processes. Using Comsol, we were able to accurately simulate mouse thermoregulatory profiles during heat exposure and 20 h of recovery. The thermoregulation model of the mouse shown here was used to reset the T_c recovery profiles under heat stress by GA optimizer.

We presented a novel function that simulated the thermoregulation using an error integrator between T_{set} and T_c. The error integration action that manipulated the metabolic activity was motivated both by early observation that the depth and duration of the hypothermia is directly related to the heat severity (12), and to maintain an offset-free thermoregulation. Although the model was able to predict the depth of hypothermia and recovery times fairly well, fever during the second day of recovery was not accurately simulated. Current data on post-heat stress T_c elevations suggest that fever occurs in response to endotoxin leakage across damaged gut epithelial membranes following thermal injury (11). Endotoxemia causes inflammation in the system and subsequent production of

cytokines, which are known to mediate thermoregulatory responses (11). The morbidity and mortality associated with extreme heat stress is due to dysfunction of multiple organ systems as a consequence of the systemic inflammatory response syndrome (1). A more detailed model, including these biochemical changes, should be able to predict the fever response post-heat stress.

To accurately simulate the pre-heating period, T_{set} had to be set to 34°C, and then changed to 36.35°C for the rest of the simulation. The change in T_{set} corresponds to the thermoregulatory observation in small rodents and is successfully predicted by the mathematical model. There is evidence that a hidden set point of a unified system is unnecessary, and coordination between thermoeffectors is achieved through their common controlled variable, body temperature (19). However, in the present work, a simplification was introduced to describe more detailed body thermoregulation.

Developing effective pharmacological treatments for HS recovery will probably require relatively demanding multidisciplinary research of the biochemical changes occurring at the cellular level. On the other hand, examining the influence of T_a upon the recovery of animal models from HS conditions is a relatively simpler assignment. Currently, HS is being treated by rapid cooling therapy. However, while a rapid reduction of body temperature is efficacious following HS collapse, when body temperature is still elevated, efficacious treatments during ensuing hours and days of recovery have yet to be identified. The relatively detailed three-dimensional Comsol simulation model enabled us to determine the efficacy of various T_a treatment strategies for HS recovery. A GA optimization was conducted to minimize the offset in T_c during the recovery period using eight time segments of 110 min. The GA optimization solution predicts that using $T_a = 27$°C for the initial 110 min of recovery, followed by $T_a = 30, 31, 29, 28, 28, 27$, and 26°C for the rest of the segments, resulted in a 7-h hypothermia duration, which represented a reduction of 58% compared with a 12-h hypothermia duration at a constant T_a of 25°C. The in silico model developed in the present study indentifies a series of T_a values that can be used to reestablish T_{set} following HS. However, hypothermia may be a thermoregulatory response that permits survival following HS, disruption of which is detrimental under some conditions (12). The factor 10 in *Eq. 11* was chosen to emphasize the importance of reducing the body temperature as fast as possible. There is no obvious guidance for the size of the factor, and different factors could create slightly different results. However, the solution that was generated suggests rapid cooling after the heat stress conditions. This would likely be generated by a larger factor as well.

The GA is a stochastic optimization method that has its share of drawbacks; however, understanding the nature of the specific optimization problem and the lack of gradient-based information lead us to choose the GA optimization over other alternatives. A gradient-based optimization would lead to a large number of evaluations of the Comsol model that would take an unreasonable amount of time. Moreover, this highly nonlinear optimization will be very sensitive to the initial conditions, and this may lead to a yet larger number of optimizations. The GA provides the ability to conduct a search on a relative rough grid of temperatures to indicate a proof of concept showing the ability of a simulation to predict a nontrivial treatment.

The model presented is a simplification of reality. The geometry of the real mouse body was simplified. The metabolic regulation by an integrator controller mechanism is a hypothesis that could incorporate a statistical behavior of more complicated regulation mechanisms in reality. We based the metabolic heat generation on Kleiber's law, and this could lead to some inaccuracies when used across species, and, indeed, we needed to multiply the metabolic heat generation by a factor of three to enable thermoregulation.

All mathematical models are an approximation of reality; therefore, despite the many advantages of using these models, one has to take into account the limitations. In the discussion, model simplification of the morphology of the mouse was done, the blood system, the nervous system signals, and also the heat loss through the respiratory system were neglected. Moreover, during heat stress, small rodents adjust body temperature on a hyperthermic plateau. The height of the plateau depends on salivation threshold, which is also affected by T_a. This mechanism was neglected and could be taken into consideration in future versions of the model. Despite numerous approximations, the model is enough to provide accurate predictions of mouse body temperature distribution as a result of changing environmental conditions.

The model presented here demonstrates the usefulness of in silico research in designing novel hypotheses that can be tested in vivo. Substantial regarding the computer model in terms of HS, in silico data can be of significant benefit in narrowing the identification of regulatory windows that may prove efficacious in treatment of HS patients. Testing the computer model via multiple iterations, complemented by the inclusion of new in vivo data, offers a powerful experimental tool to significantly enhance the discovery of novel therapeutic strategies. Consistent with the use of a systems biology approach, combining in vitro, in vivo, and in silico models holds significant promise in reducing animal use, as well as the ambiguity associated with experimental protocols consisting of a large number of variables.

DISCLOSURES

No conflicts of interest, financial or otherwise, are declared by the author(s).

REFERENCES

1. **Bouchama A, Knochel JP.** Heat stroke. *N Engl J Med* 346: 1978–1988, 2002.
2. **Charny CK, Hagmann MJ, Levin RL.** A whole body thermal model of man during hyperthermia. *IEEE Trans Biomed Eng* 34: 375–387, 1987.
3. **Dematte JE, O'Mara K, Buescher J, Whitney CG, Forsythe S, McNamee T, Adiga RB, Ndukwu IM.** Near-fatal heat stroke during the 1995 heat wave in Chicago. *Ann Intern Med* 129: 173–181, 1998.
4. **Elia M.** Organ and tissue contribution to metabolic rate. In: *Energy Metabolism Tissue Determinants and Cellular Corollaries*, edited by Kinney JM and Tucker H. New York: Raven, 1992, p. 61–77.
4a. **Fan L, Hsu F, and Hwang C.** A review on mathematical models of the human thermal system. *IEEE Trans Biomed Eng* 18: 16, 1971.
5. **Fiala D, Lomas KJ, Stohrer M.** A computer model of human thermoregulation for a wide range of environmental conditions: the passive system. *J Appl Physiol* 87: 1957–1972, 1999.
6. **Goldman L, Ausiello DA.** *Cecil Medicine.* Philadelphia, PA: Saunders Elseiver, 2007.

7. **Gordon CJ** *Temperature Regulation in Laboratory Rodents*. Cambridge, UK: University Press, 1993.
8. **Grosman B, Lewin DR.** Adaptive genetic programming for steady-state process modeling. *Comput Chem Eng* 28: 2779–2790, 2004.
9. **Havenith G.** Individualized model of human thermoregulation for the simulation of heat stress response. *J Appl Physiol* 90: 1943–1954, 2001.
10. **Holland JH.** *Adaptation in Natural and Artificial Systems*. Ann Arbor, MI: University of Michigan Press, 1975.
11. **Leon LR, Blaha MD, DuBose DA.** Time course of cytokine, corticosterone, and tissue injury responses in mice during heat strain recovery. *J Appl Physiol* 100: 1400–1409, 2006.
12. **Leon LR, DuBose DA, Mason CW.** Heat stress induces a biphasic thermoregulatory response in mice. *Am J Physiol Regul Integr Comp Physiol* 288: R197–R204, 2005.
13. **Leon LR, Gordon CJ, Helwig BG, Rufolo DM, Blaha MD.** Thermoregulatory, behavioral, and metabolic responses to heatstroke in a conscious mouse model. *Am J Physiol Regul Integr Comp Physiol* 299: R241–R248, 2010.
14. **Leon LR, Walker LD, DuBose DA, Stephenson LA.** Biotelemetry transmitter implantation in rodents: impact on growth and circadian rhythms. *Am J Physiol Regul Integr Comp Physiol* 286: R967–R974, 2004.
16. **Martens WJ.** Climate change, thermal stress and mortality changes. *Soc Sci Med* 46: 331–344, 1998.
17. **Pennes HH.** Analysis of tissue and arterial blood temperatures in the resting human forearm. *J Appl Physiol* 1: 93–122, 1948.
18. **Pisacane VL, Kuznetz LH, Logan JS, Clark JB, Wissler EH.** Thermoregulatory models of space shuttle and space station activities. *Aviat Space Environ Med* 78: A48–A55, 2007.
19. **Romanovsky AA.** Thermoregulation: some concepts have changed. Functional architecture of the thermoregulatory system. *Am J Physiol Regul Integr Comp Physiol* 292: R37–R46, 2007.
20. **Schmidt-Nielsen K, Hainsworth FR, Murrish DE.** Counter-current heat exchange in the respiratory passages: effect on water and heat balance. *Respir Physiol* 9: 263–276, 1970.
21. **Stitt JT.** Fever versus hyperthermia. *Fed Proc* 38: 39–43, 1979.
22. **Trakic A, Liu F, Crozier S.** Transient temperature rise in a mouse due to low-frequency regional hyperthermia. *Phys Med Biol* 51: 1673–1691, 2006.
23. **Wainwright PR.** The relationship of temperature rise to specific absorption rate and current in the human leg for exposure to electromagnetic radiation in the high frequency band. *Phys Med Biol* 48: 3143–3155, 2003.
24. **Wang Z, O'Connor TP, Heshka S, Heymsfield SB.** The reconstruction of Kleiber's law at the organ-tissue level. *J Nutr* 131: 2967–2970, 2001.
25. **Waterhouse J, Drust B, Weinert D, Edwards B, Gregson W, Atkinson G, Kao S, Aizawa S, Reilly T.** The circadian rhythm of core temperature: origin and some implications for exercise performance. *Chronobiol Int* 22: 207–225, 2005.
26. **Wooden K, Walsberg G.** Effect of wind and solar radiation on metabolic heat production in a small desert rodent, *Spermophilus tereticaudus*. *J Exp Biol* 203: 879–888, 2000.